A Computational Investigation into the Effect of Infarction on Clinical Human Electrophysiology Biomarkers

Louie Cardone-Noott[1], Alfonso Bueno-Orovio[1], Ana Mincholé[1], Kevin Burrage[1,2], Mikael Wallman[1,3], Nejib Zemzemi[4], Erica Dall'Armellina[1,5], Blanca Rodriguez[1]

[1] University of Oxford, Oxford, UK
[2] Queensland University of Technology, Brisbane, Australia
[3] Fraunhofer-Chalmers Centre, Gothenburg, Sweden
[4] INRIA Bordeaux Sud-Ouest, Bordeaux, France
[5] Oxford University Radcliffe Department of Medicine, Oxford, UK

Abstract

The electrocardiogram (ECG) is often used to diagnose myocardial infarction, but sensitivity and specificity are low. Here we present a computational framework for solving the bidomain equations over an image-based human geometry and simulating the 12 lead ECG. First, we demonstrate this approach by evaluating a population of eight models with varying distributions of local action potential duration, and report that only the model with apicobasal and inter-ventricular heterogeneities produces concordant T waves. Second, we simulate the effects of an old anterior infarct, which causes a reduction in T wave amplitude and width. Our methodology can contribute to the understanding of ECG alterations under challenging conditions for clinical diagnosis.

1. Introduction

The electrocardiogram (ECG) is frequently used as a first-line tool to diagnose myocardial infarction (MI), but the sensitivity of the ECG to acute MI is only around 55% [1], and it provides limited information on the location, extent, and stage of injury. Computational studies have recently been able to simulate the activity of the heart up to the body surface, solving the so-called forward problem of electrophysiology [2]. Such studies are uniquely able to test hypotheses by merit of their flexibility and the high spatio-temporal resolution datasets they provide.

The aim of this study is to investigate the effect of pathological conditions on the ECG by solving the forward problem of electrocardiography, with consideration given to inter-subject variability. In order to achieve this, we develop an image-derived human heart-torso model, including a detailed description of human ventricular electrophysiology. The ECG morphology is the result of dispersion of local activation and repolarisation times. These quantities are difficult to measure, and highly variable between individuals. Using this realistic model we explore the impact of the different electrophysiological heterogeneities reported experimentally in order to recreate representative human ECGs under healthy conditions. We then present simulation results of the effect of scar regions on the ECG.

2. Methods

2.1. Electrical conduction model

We model the electrical activity in the heart with the bidomain equations [3]. Physically the bidomain model describes a region containing intracellular and extracellular electric fields. The equations are coupled to a model of cardiac cellular activity at the nodes through the transmembrane voltage (the difference between the fields).

Outside of the heart the electrical potential is governed by the Laplace equation. The torso potential is coupled to the extracellular potential in the heart, and the bidomain-torso system solved monolithically. We calculate the 12-lead ECG by recording the extracellular potential at the standard electrode positions.

2.2. Anatomical model

We used a human heart mesh [4] truncated at the base below the valves, resulting in a bi-ventricular geometry. The mesh was generated with an edge length of 0.4 mm, and contains 2.51 million nodes and 14.2 million tetrahedral elements. Fibre structure was generated using a rule-based method to replicate the findings of Streeter et al. [5].

Orthotropic intracellular conductivities were chosen such that the conduction velocities (CVs) were close to

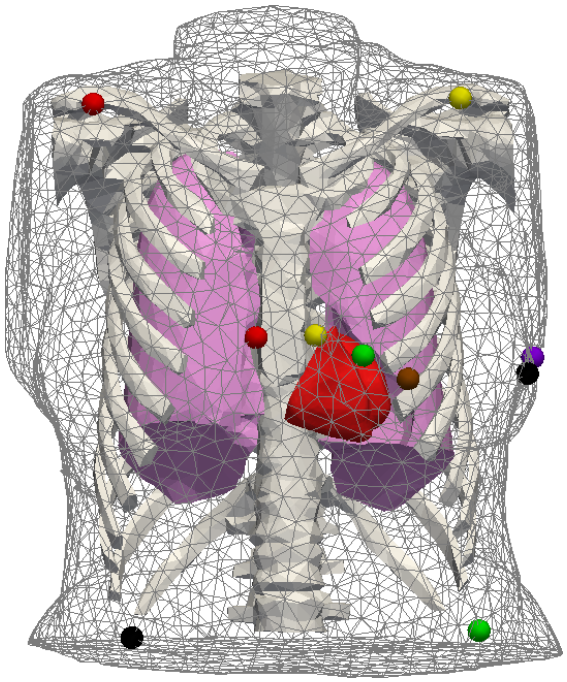

Figure 1. A visualisation of the combined heart-torso mesh. The coloured spheres indicate the location of the "electrodes" using standard (European) colour-coding.

67, 30, and 17 cm/s in the fibre, sheet, and inter-sheet directions respectively, as measured in pig ventricles [6] (specifically 1.5, 0.45, and 0.225 mS/cm). Axisymmetric extracellular conductivities were used based on measured resistivity ratios [7], specifically 5.46 and 2.03 mS/cm in the fibre and transverse directions respectively.

The biventricular mesh was embedded in a torso geometry generated from CT images of a 43 year old woman. The DICOM images were segmented using the medical imaging software Osirix into lung, bone, and the rest. These surfaces were meshed using INRIA meshing Software MMG3D. The combined mesh (fig. 1) has a total of 3.25 million nodes and 19.4 million tetrahedra. We assigned isotropic conductivities of 0.389 and 0.2 mS/cm to the lung and bone elements respectively [8], and 2.16 mS/cm in the rest (a human trunk measurement [9]).

2.3. Electrophysiological heterogeneities

Dispersion of action potential duration (APD) has been reported in three orientations: transmural (across the ventricle wall), apico-basal (apex to base), and interventricular (between left and right ventricles) [10,11]. In the following we describe how we constructed each of these gradients.

In all cases we used the 2006 human ventricular model of ten Tusscher and Panfilov (TT06) [12], and adjusted only the delayed rectifier potassium current (g_{Ks}). A larger value of g_{Ks} leads to a shorter APD, and *vice versa*. As a control we used a homogeneous (HOM) case with the published endocardial model everywhere.

Transmural (TM): Endocardial APD is longer than epicardial (by 62 ms [13]). We modelled this by making use of the published TT06 parameter sets. The outer 40% of the heart wall was assigned the epicardial model, and the inner 60% the M-cell model. We chose the M-cell model over the endocardial one as the APD of the endo- and epicardial models are similar (286 and 292 ms respectively), but the APD of the M-cell model is longer (354 ms). This choice was only made to better replicate the reported APD dispersion in the human ventricular wall.

Apicobasal (AB): Apex-to-base dispersion of activation-recovery interval (ARI, a surrogate for APD) has been measured noninvasively in human as 42 ms [14] (mean of 7 subjects) with shorter ARI at the apex than the base. Experiments with canine and human tissue samples suggest the same [15]. We modelled this gradient by increasing g_{Ks} by 50% of normal at the apex.

Interventricular (IV): APD is longer in the LV than the RV [16]. ARI dispersion between the ventricles was 32 ms for one subject in [14] with longer ARI in the LV than the RV. We modelled this by increasing g_{Ks} in the RV and decreasing it in the LV, both by 15% of normal.

For the combined systems, the above rules were simply applied together. In total we evaluated all eight combinations of heterogeneities (including HOM).

2.4. Scar generation

We assigned regions of scar by first manually approximating the ventricular volume in direct contact with the left anterior descending (LAD) artery, since occlusion of this artery is a frequent cause of infarction. Within this area, a number of contact points were selected, corresponding to the actual sites where the LAD branches penetrate the ventricles. The number of contact points may be chosen at random, allowing for various types of scars, ranging from solid patches of non-conductive tissue to fractionated structures containing channels of viable tissue. Next, each contact point was associated with a radial basis function, and tissue below a threshold in the basis support was labelled as infarct (3.4% of the total, fig. 2). Scar volume may be increased or decreased by altering the threshold.

We included an infarct as an unexcitable region with reduced conductivity. Within the scar region, intracellular conductivity was reduced to 0 and all ion activity removed, and extracellular conductivity was decreased to one third of the normal values, resulting in approximately a 50% reduction in CV, as reported in rabbit [17]. The area immediately surrounding the scar (15.5% of all nodes) became a "border zone" of slower-conducting but otherwise normal tissue. Here both intracellular and extracellular conduc-

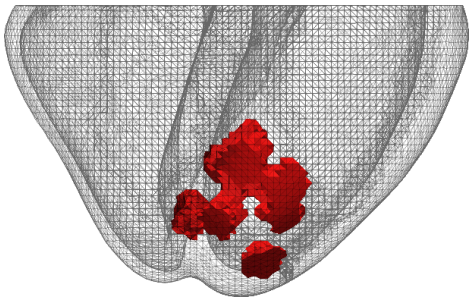

Figure 2. A visualisation of the infarct region simulated in this work, shown in red. The region is mainly in the anterior apical septum.

tivities were reduced by two thirds, again reducing CV by about half.

2.5. Activation sequence

A beat was initiated with five simultaneous stimuli (four in the left ventricle and one in the right ventricle) corresponding to locations of earliest activation measured in an isolated human heart [18]. Because of the uncertainties in constructing an anatomically detailed activation network, the general effect of the Purkinje system in coordinating activation throughout the ventricles was included by increasing the intracellular conductivity tensors of all elements on both endocardial surfaces. These conductivity tensors were made isotropic with magnitude 16.75 mS/cm yielding a conduction velocity close to the 2.2 m/s reported for Purkinje fibres [19].

2.6. Computational techniques

All simulations were performed with Chaste [20] on the Archer supercomputer (a Cray XC30 system composed of 3,008 compute nodes, each containing two 2.7 GHz 12-core Intel E5-2697 v2 processors, and 64 GB of memory). The bidomain PDEs were solved using the finite element method and PETSc with a time step of 40 μs. The TT06 ODEs were solved using CVODE with adaptive time step. 500 ms of simulation typically took about 2 hours on 20 nodes (480 threads of execution).

3. Results and Discussion

The eight systems described above resulted in a range of morphologies in the ECG leads, shown for the V2 lead (yellow sphere in fig. 1) for brevity in fig. 3. The left plot shows the four systems that generated a normal, positive T-wave in this particular lead; the right plot abnormal T waves in this lead. The AB and IV modifications to g_{Ks} had no effect on the QRS complex, but the presence of different cell models transmurally reduced its amplitude and increased its width slightly. With this activation protocol and choice of electrodes, only the system with apico-basal and interventricular heterogeneities generated T waves with no abnormalities in any of the twelve leads.

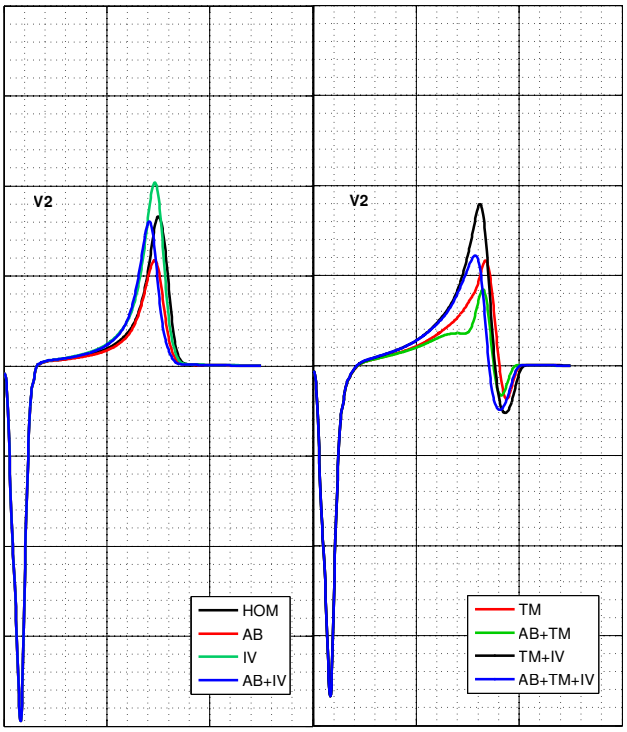

Figure 3. Lead V2 for eight APD distributions. Four generated positive T waves (left), four generated biphasic or "camel hump" T waves (right). The grid is the same as standard ECG paper (200 ms/0.5 mV large squares).

This system (AB+IV) was further investigated in the presence of scar injury. The V2 lead is newly shown in fig. 4, with the normal result for comparison. The scar case depicts a reduced QRS amplitude and narrower T wave width.

The 12 lead ECG is a highly compressed representation of activation and repolarisation in the heart. Consequently, when attempting to find parametrisations that result in a given ECG shape, there are many possibilities (figs. 3). Of the eight systems tested only one (AB+IV) had qualitatively normal T waves in all leads.

The results for anterior infarction (fig. 4) are promising, displaying reduced QRS and T wave amplitudes and widths, possibly due to the reduction in excitable tissue volume. However the QRS normally widens in infarcted hearts. This may be because such hearts are usually ischaemic, a pathology not yet included in the model. Future research will improve the model of myocardial tissue affected by coronary occlusion, and further develop the methodology as a potential diagnostic tool.

Figure 4. The V2 lead for the system with AB and IV heterogeneities, with and without scar and border zone.

Future investigations will also concentrate on the improvement of several methodological challenges. First, our activation sequence requires optimisation to better orient the ECG axis. Second, the geometry is made up of two parts from different acquisitions and volunteers, and manually aligned. Third, validation of simulation results is challenging due to the large inter-subject variability in human ECG recordings.

Acknowledgements

LCN is funded by the EPSRC Systems Biology Doctoral Training Centre. AM holds a Marie Curie Intra-European Fellowship. ABO and BR are supported by BR's Wellcome Trust Senior Research Fellowship in Basic Biomedical Sciences. This work used the ARCHER UK National Computing Service (http://www.archer.ac.uk).

References

[1] Fesmire FM, *et al*. Usefulness of automated serial 12-lead ECG monitoring during the initial emergency department evaluation of patients with chest pain. Ann Emerg Med 1998;31:3–11.

[2] Zemzemi N, *et al*. Computational Assessment of Drug-Induced Effects on the Electrocardiogram: From Ion Channel to Body Surface Potentials. Brit J Pharmacol 2012;168:718–733

[3] Tung L. A bi-domain model for describing ischemic myocardial D-C potentials. Dept. of Electr. Eng. and Comput. Sc., MIT, 1978

[4] Sebastian R, *et al*. Assessing influence of conductivity in heart modelling with the aim of studying cardiovascular diseases. In Proceedings of SPIE 2008;691627:1–10.

[5] Streeter DD, *et al*. Fiber orientation in the canine left ventricle during diastole and systole. Circ Res 1969;24:339–347.

[6] Caldwell BJ, *et al*. Three distinct directions of intramural activation reveal nonuniform side-to-side electrical coupling of ventricular myocytes. Circ Arrhythm Electrophysiol 2009;2:433–440.

[7] Clerc L. Directional differences of impulse spread in trabecular muscle from mammalian heart. J Physiol 1976;255:335–346.

[8] Gabriel S, *et al*. The dielectric properties of biological tissues: III. parametric models for the dielectric spectrum of tissues. Phys Med Biol 1996;41:2271.

[9] Rush S, *et al*. Resistivity of body tissues at low frequencies. Circ Res 1963;12:40–50.

[10] Roberts BN, *et al*. Computational approaches to understand cardiac electrophysiology and arrhythmias. Am J Physiol Heart Circ Physiol 2012;303:H766–H783.

[11] Burton FL, Cobbe SM. Dispersion of ventricular repolarization and refractory period. Cardiovasc Res 2001;50:10–23.

[12] ten Tusscher KHWJ, Panfilov AV. Alternans and spiral breakup in a human ventricular tissue model. Am J Physiol Heart Circ Physiol 2006;291:H1088–H1100.

[13] Näbauer M, *et al*. Regional differences in current density and rate-dependent properties of the transient outward current in subepicardial and subendocardial myocytes of human left ventricle. Circulation 1996;93:168–177.

[14] Ramanathan C, *et al*. Activation and repolarization of the normal human heart under complete physiological conditions. PNAS 2006;103:6309–6314.

[15] Szentadrassy N, *et al*. Apico–basal inhomogeneity in distribution of ion channels in canine and human ventricular myocardium. Cardiovasc Res 2005;65:851–860.

[16] Bueno-Orovio A, *et al*. In vivo human left-to-right ventricular differences in rate adaptation transiently increase pro-arrhythmic risk following rate acceleration. PLoS ONE 2012;7:e52234.

[17] Walker NL, *et al*. Mapping of epicardial activation in a rabbit model of chronic myocardial infarction. J Cardiovasc Electrophysiol 2007;18:862–868.

[18] Durrer D, *et al*. Total Excitation of the Isolated Human Heart. Circulation 1970;6:899–912.

[19] Draper MH, Weidmann S. Cardiac resting and action potentials recorded with an intracellular electrode. J Physiol 1951;115:74–94.

[20] Mirams GR, *et al*. Chaste: An open source C++ library for computational physiology and biology. PLoS Comput Biol 2013;9:e1002970.

Address for correspondence:

Mr. Louie Cardone-Noott
Linacre College, Oxford, OX1 3JA, UK
louie.cardone-noott@cs.ox.ac.uk